Structure, Optical and Magnetic behavior of $LaFeO_3$ and $LaFe_{0.9}Ni_{0.1}O_{3-u}$ by combustion method.

C. Jagadeeshwaran, A. Paul Blessington Selvadurai, V. Pazhanivelu, R. Murugaraj.
Department of Physics,
Anna University, Chennai-600 025, India.
r.murugaraj@gmail.com.

Abstract— **In the present work, we report the pure $LaFeO_3$ and Nickel doped ($LaFe_{0.9}Ni_{0.1}O_{3-u}$:1samples for tunable optical and magnetic properties. The samples were prepared by citrate combustion method. This method offers us a very rapid synthesis of the samples. Prepared samples were kept in hot plate to initiate the combustion process. Samples were grounded and calcined in furnace at $800^O C$ for 2 Hrs. The XRD analysis confirms the phase formation of $LaFeO_3$ and Ni doped $LaFeO_3$. The local structure of these samples was studied using Raman spectroscopy. Raman analysis shows, Ni^{2+} doping effect on the tilt and stretching phonon modes of $LaFeO_3$. SEM picture shows fine grains were grown with random shapes. Optical measurements were done using a U-V visible spectrometer. The Ni^{2+} ion doping significantly broadens the absorption regions. The enhancement of room temperature magnetization value is observed from the M-H curve measured using VSM. Thus, the optical and magnetic properties were significantly influenced by Ni^{2+} doping and can be tuned for functional device applications.**

Keywords: citrate precursor, Combustion, XRD, Raman Spectroscopy, Magnetization, Optical absorption

I. INTRODUCTION

In the present, recent years, ABO_3 perovskite-type materials are more attractive and important, since these materials have a great potential, which contribute to several fields of research interest such as solid fuel cell, solid electrolyte, fixed resistor, actuators, electromechanical devices, transducers, etc., because of special crystal structure, magnetism, electric conductivity, piezoelectric and electro-optic properties, catalytic activity and gas sensitivity, etc. [1, 2, 3]. Conventional synthesis of solid state reaction used equimolar oxide mixing and grinding periodically to get a dense single phase, this method needs a high calcination temperature (1100–1300 °C) for the reaction to occur and often results in the formation of coarse aggregates, which are difficult to break down. The grain size of the product obtained by this method is relatively large making it unsuitable for some applications, particularly for the application of photo catalytic material. Though there are several popular methods of reaction to prepare fine nano grains, mechanochemical solid reaction, sol–gel, hydrothermal synthesis, sonochemical synthesis, thermal decomposition of the heteronuclear complex, wet chemically coprecipitation, a polymerizable complex method and a microemulsion method. In which decomposition of sol gel by combustion method, particularly citrate decomposition method is a really well recognized method of synthesizing ABO_3 compound in a lesser time consumption [4] which was reported for numerous compounds AB_2O_4 and ABO_3. Also preparation of different nanostructure is reported by using this method [5]. From the literature, we observed that most of the reports of Ni doping were reported by solid state reaction method [6-8]. We observe a scarce literature of Ni doping prepared by citrate combustion method. Thus the present work, we have synthesized the $LaFeO_3$ and $LaFe_{0.9}Ni_{0.1}O_{3-\delta}$ to develops and enhances the optical and magnetic properties prepared by citrate combustion method.

II. EXPERIMENTAL

Analytical grade $Fe(NO_3)_3 \cdot 9H_2O$, $Ni(NO_3)_2 \cdot 6H_2O$, La_2O_3 and $C_6H_8O_7 \cdot H_2O$ were used as raw materials to prepare $LaFeO_3$ and $LaFe_{0.9}Ni_{0.1}O_{3-\delta}$. $La(NO_3)_3 \cdot xH_2O$ were prepared by dissolving the La_2O_3 in Dil.HNO_3. The reaction was processed as reported [4]. X-ray diffractometer (XRD) analysis for all samples were done with Bruker D2 Phaser a Bench top model using Cu K$_1$ radiation. SEM image was recorded by using the instrument Quanta 200 FEG. The Optical studies were performed by measuring the absorbance in the wavelength region =300–800 nm at room temperature using UV–Vis spectrophotometer (Shimadzu UV 2450 PC Spectrophotometer). The magnetic analysis was done using vibrating sample magnetometer VSM Lakeshore - 7410.

III. XRD ANALYSIS

Figure 1 shows the XRD pattern of $LaFeO_3$ and $LaFe_{0.9}Ni_{0.1}O_{3-\delta}$. The XRD pattern confirms $LaFeO_3$ phase and the presence of Ni dopant in the sample. The observed patterns all indexed with JCPDS card no.37-1493. The lattice parameter of the samples was found by using the GSAS software by Reitveld method with a space group of Pbnm (#62). The observed lattice parameter, increase on Ni doping and this confirms that the valence state of nickel is in Ni^{2+}. Since, Ni^{3+} in $LaFeO_3$ usually decreases the lattice parameter on substitution[6]. The lattice parameter values obtained from the profile fit for $LaFeO_3$ and $LaFe_{0.9}Ni_{0.1}O_{3-\delta}$ are a=5.548 Å, b=5.556 Å and c=7.843Å and a= 5.551 Å, b=5.558 Å and c=7.846 Å correspondingly. We observe no other secondary phases and this may be either the obtained material could be of single phase or the secondary phase could not be detected from the XRD due to the limitation in the detection. We have measured the average crystallite size using Williamson-Hall plot, given below in the equation (1). Where D is the particle size in nanometers, is the wavelength of the radiation (1.54056 Å for CuK radiation), k is a constant equal to 0.94, $_{1/2}$ is the peak width at half-maximum intensity and is the peak position.

$$\beta_{1/2}Cos_{\theta} = \frac{K\lambda}{D} + 4\nu \sin_{\theta} \tag{1}$$

The average crystallite size calculated from it shows that the crystallite size are in nano region; size of the crystallite measured for $LaFeO_3$ and $LaFe_{0.9}Ni_{0.1}O_{3-\delta}$ are 55 nm and the micro strain values are 1.8×10^{-4}. Both samples exhibit only a compressive strain indicated by a negative slope which is shown in the inset of Figure 1, as fitted by the straight line equation. Compressive strain behavior is due to the nano size effect [9], because of the shrinkage of the lattice parameter.
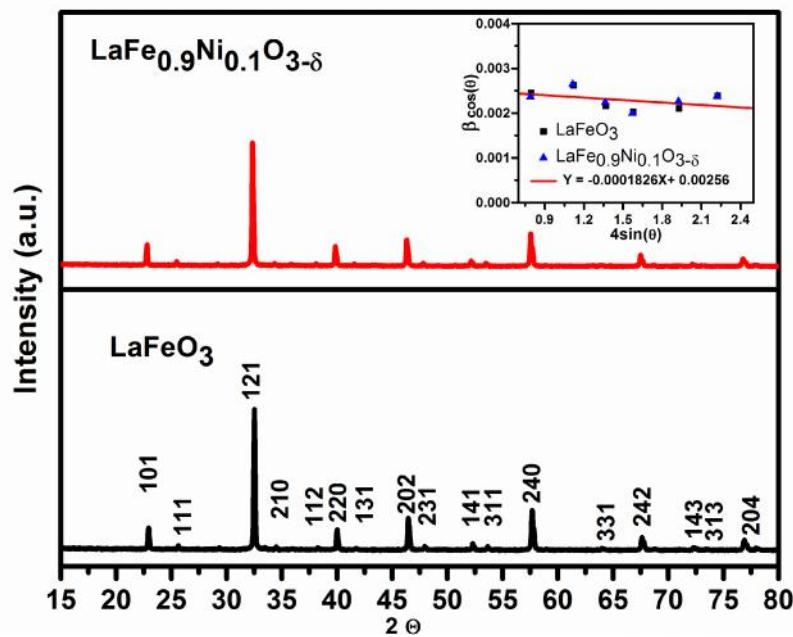

Figure 1. XRD pattern of $LaFeO_3$ and $LaFe_{0.9}Ni_{0.1}O_{3-u}$

IV. SEM ANALYSIS

SEM images of Figure 2 show the local morphological of $LaFeO_3$ and $LaFe_{0.9}Ni_{0.1}O_{3-\delta}$, images show a well nano crystalline grains, agglomerated with random shapes, closely signifying the spherical signature of the particles, particularly for $LaFe_{0.9}Ni_{0.1}O_{3-\delta}$ SEM images. SEM images of $LaFeO_3$ show distributed size of grains are present in it, which are comparatively larger than the grain size of $LaFe_{0.9}Ni_{0.1}O_{3-\delta}$. We see that the measured grain sizes are relatively remains same to the crystallite size, measured from the XRD and deviation in crystallite size is expected. Since, XRD measures the average crystallite size over the region of focus of the X-ray source, similarly SEM does it.
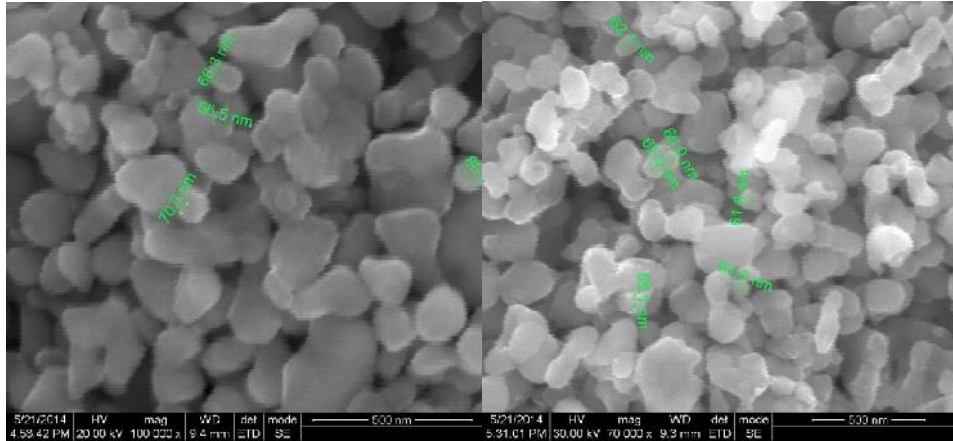
Figure 2. SEM picture of LaFeO₃ and LaFe₀.₉Ni₀.₁O₃₋ᵤ
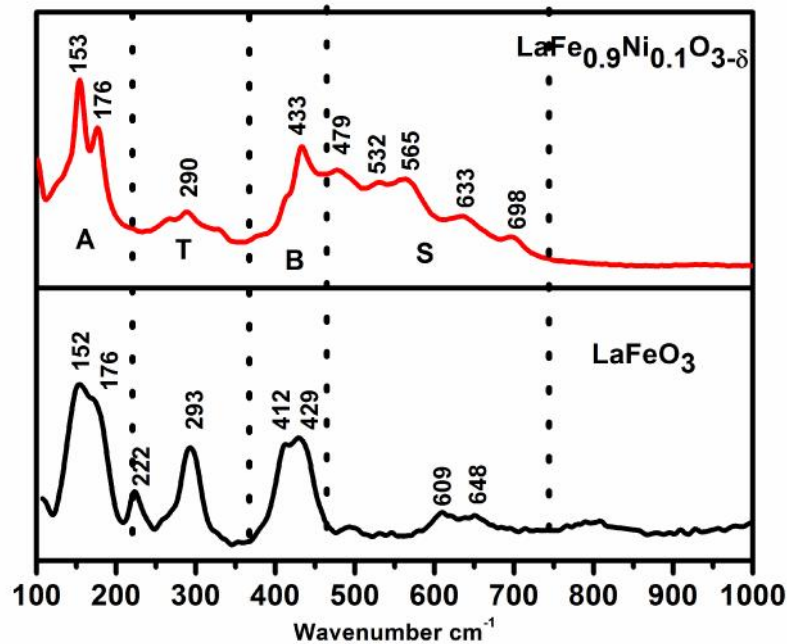
V. RAMAN ANALYSIS

Figure 3. Raman spectra of LaFeO₃ and LaFe₀.₉Ni₀.₁O₃₋ᵤ|

The crystals of $LaFeO_3$ have an orthorhombically distorted pervoskite structure with space group D^{16}_{2h} (Pbnm) with four formula units per unit cell. According to the group theory analysis that the Brillion zone center normal modes transform according to the representation [10].

$$7A_g \oplus 8A_u \oplus 5B_{1g} \oplus 10B_{1u} \oplus 7B_{2g} \oplus 8B_{2u} \oplus 5B_{3g} \oplus 10B_{3u} \qquad (2)$$

The representation $A_u \oplus 2B_{1u}$ belongs to three acoustic modes. Modes A_g, B_{1g}, B_{2g} and B_{3g} are Raman active and modes A_u, B_{1u}, B_{2g}, B_{2u}, B_{3g} and B_{3u} are infrared active. Based on this analysis, one expects 24 Raman active modes. Raman spectra were recorded using 785 nm laser diode. The modes were measured between the regions of 1000 cm⁻¹ -100 cm⁻¹ shown in Figure 3. Generally the Modes caused by La vibrations are present below 200 cm⁻¹, labeled (A). Modes between 200 and 300 cm⁻¹ are oxygen octahedral tilt modes (T) in La. Modes between 400 cm⁻¹ and 450 cm⁻¹ are oxygen octahedral bending vibrations (B) and modes above 500cm⁻¹ are oxygen stretching vibrations (S) [11]. It is seen from the spectra that Ni^{2+} doping affects the

Oxygen tilt, stretching and bending modes of vibration. The spectra of $LaFeO_3$ and $LaFe_{0.9}Ni_{0.1}O_{3-\delta}$ are distinct by each other, the appearance and disappearance of phonon modes i.e., the peak at 222 cm^{-1} is present in $LaFeO_3$, but not in $LaFe_{0.9}Ni_{0.1}O_{3-\delta}$ several other shoulder peaks are seen in $LaFe_{0.9}Ni_{0.1}O_{3-\delta}$ in the oxygen stretching modes. From the literature there are discrepancies in observing the phonon modes for $LaFeO_3$ from the spectra observed or reported [11- 14]. It is seen that the intensity and the peak position observed are varied on their measurements; the observed modes are mostly A_g and B_{2g} modes, these are excitable in the a-c plane of the materials, orientation of these planes make the laser spot to measure average scattering of modes, which suggest that domain orientation influence the both intensity and peak position [15].
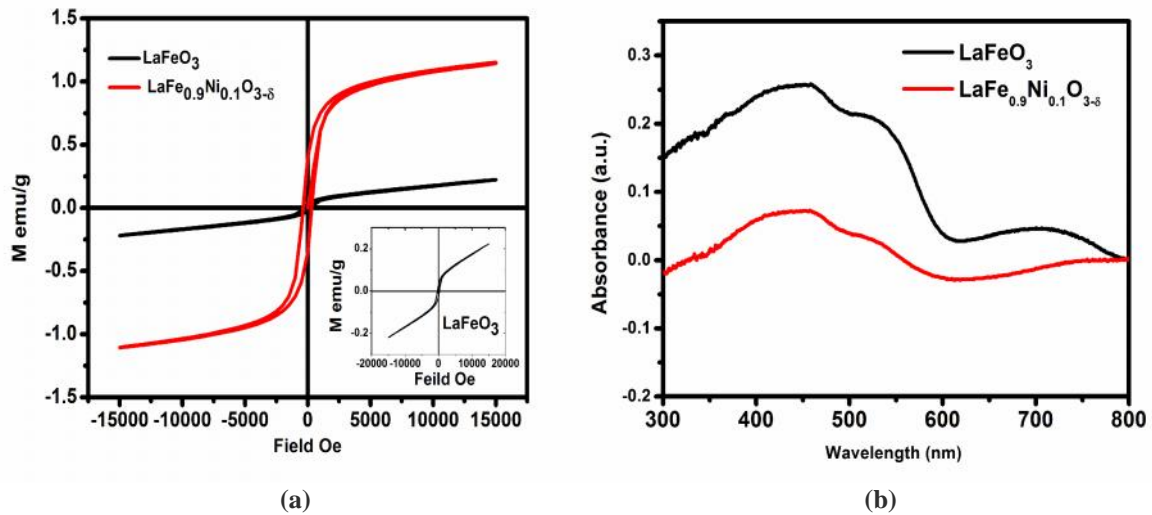
VI. MAGNETIC AND OPTICAL ANALYSIS

(a)   **(b)**

Figure 4. M-H and optical curve of $LaFeO_3$ and $LaFe_{0.9}Ni_{0.1}O_{3-u}$

Figure 4a of The M-H curve shows the Isothermal M-H curve of $LaFeO_3$ and $LaFe_{0.9}Ni_{0.1}O_{3-\delta}$, observed magnetization parameters are given in the table.1. It is seen that the $LaFeO_3$ show weak ferromagnetism shown in the inset of Figure 5. The origin of this magnetization is due to the canted spin present on the surface of the nanoparticles. The observed M-H curves are biased due to the presence of both ferro and anti ferromagnetic phase present in the sample. The sample show a negative exchange bias, were the loops are represent with coercivity of H_{c+} and H_{c-} in the M-H curve. We have estimated H_{EB} and H_C from the well known relations, H_{EB} = -(H_{c+} + H_{c-})/2 and H_C = (H_{c+} - H_{c-})/2, respectively are given in table 1. Enhanced magnetization is observed in the case of Ni^{2+} doping, this may be due to the uncompensated spin present of Ni^{2+} in the Fe^{3+} site [8]. From the magnetization curve it is seen that the both ferro and antiferromagnetism coexist i.e. at high field the M-H curve does not saturate.

Table.1 M-H curve parameters of $LaFeO_3$ and $LaFe_{0.9}Ni_{0.1}O_{3-ul}$

Samples	Mr emu/g	H_{c+} Oe	H_{c-} Oe	Hc Oe	H_{ex} Oe
$LaFeO_3$	0.03	256	310	283	27
$LaFe_{0.9}Ni_{0.1}O_{3-u}$	0.4	314	367	340.5	26.5

Figure 4b of optical curve shows the UV–Vis absorption spectra of $LaFeO_3$ and $LaFe_{0.9}Ni_{0.1}O_{3-\delta}$. The samples have shown a strong absorption in the region of the ultraviolet (300–400 nm) and visible light region (400–800 nm). Direct band gap energy (Eg) was determined by fitting the absorption data to the direct transition as equation $ah\nu = A(h\nu-Eg)^{1/2}$, where a is the optical absorption coefficient, $h\nu$ is the photon energy, Eg is the direct band gap, and A is a constant. The extrapolation of the linear portions of the curves toward absorption equal to zero (y = 0) gives Eg for direct transitions. The observed direct band gaps of all samples were 2.1eV and 2.12 eV. These band gaps are closed to the values reported in the literature for $LaFeO_3$ [16]. Eg shows a significant shift to higher. The optical absorbance of $LaFeO_3$ is much similar to α-Fe_2O_3 [17]. Metal to ligand transition are observed between the region of 300-500 nm. These are termed as charge transfer transition, as Ni is doped, significant broadening of the Metal to ligand transition is observed, this confirm that Ni^{2+} affects the optical transition in $LaFeO_3$.

VII. CONCLUSION

$LaFeO_3$ and $LaFe_{0.9}Ni_{0.1}O_{3-\delta}$ were prepared by citrate combustion method, XRD pattern confirms the phase and the presence of Ni^{2+} in the lattice. Lattice parameter and crystallite size of the samples were determined using GSAS software and Scherrer formula. SEM image shows that the morphology of the sample is more liked spherical with grain size are randomly grown. Raman spectra of the samples show that Ni doping influences the tilting, stretching and bending vibration modes. The M-H curve illustrates the enhancement of magnetization on Ni doping. Also the optical absorption of band gap shows a broaden absorption. From the tauc plot the Ni doped band gap is blue shifted slightly.

1

REFERENCES

[1] Nandita Lakshminarayanan, John N. Kuhn, Sergey A. Rykov,Jean-Marc M. Milletc, UmitS. Ozkan "Doped $LaFeO_3$ as SOFC catalysts: Control of oxygen mobility and oxidation activity", Catal. Today 157 (2010) 446–450.

[2] Dr. Kuiying Li, Dejun Wang, Fengqing Wu, Tengfeng Xie, Tiejin Li "Surface electronic states and photovoltage gas-sensitive characters of nanocrystalline $LaFeO_3$ Mater. Chem. Phys. 64 (2000) 269–272.

[3] K.M. Parid, K.H. Reddy, S. Martha, D.P. Das, N. Biswal "Fabrication of nanocrystalline$LaFeO_3$: An efficient sol-gel auto-combustion assisted visible light responsive photocatalyst for water decomposition Int. J. Hydrogen Energy 35 (2010) 12161 - 12168.

[4] G. Shabbir, A.H. Qureshi , K. Saeed " Nano-crystalline $LaFeO_3$ powders synthesized by the citrate–gel method" Mater. Lett. 60 (2006) 3706–3709.

[5] Zhi Yang, Yi Huang, Bin Dong, Hu-Lin Li "Controlled synthesis of highly ordered $LaFeO_3$ nanowires using a citrate-based sol–gel route Mater. Res. Bull. 41 (2006) 274–281.

[6] M. Idrees, M. Nadeem , M. Siddique Role of holes states on metal to insulator transition and collapse of magnetic ordering in $LaFe_{1-x}Ni_xO_3$ (x =0.0-0.5) Curr. Appl. Phys.13 (2013)448-452.

[7] M Idrees, M Nadeem, M Mehmood, M Atif , Keun Hwa Chae and M M Hassan"Impedance spectroscopic investigation of delocalization effects of disorder induced by Ni doping in $LaFeO_3$" J. Phys. D: Appl. Phys. 44 (2011) 105401.

[8] M. Gateshki, L. Suescun, S. Kolesnik, J. Mais, K. S´wierczek, S. Short, B. Dabrowski "Structural, magnetic and electronic properties of $LaNi_{0.5}Fe_{0.5}O_3$ in the temperature range 5– 1000 K J. Solid State Chem.181 (2008) 1833– 1839.

[9] A. Khorsand Zak, W.H. Abd. Majid, M.E. Abrishami, Ramin Yousefi "X-ray analysis of ZnO nanoparticles by WilliamsonHall and size-strain plot methods" Solid State Sci. 13 (2011) 251-256.

[10] I.S. Smirnova "Normal modes of the $LaMnO_3$ Pnma phase:Comparison with La_2CuO_4 Cmca phase", Physica B 262 (1999) 247-261.

[11] M. Romero, R.W.Gómez, V.Marquina , J.L.Pérez-Mazariego, R.Escamilla "Synthesis by molten salt method of the $AFeO_3$ system (A=La, Gd)and its structural,vibrational and internal hyperfine magnetic field characterization" PhysicaB 443(2014)90–94.

[12] Monica Popa, Johannes Frantti, Masato Kakihana "Lanthanum ferrite $LaFeO_{3+d}$ nanopowders obtained by the polymerizable complex method" Solid State Ionics 154– 155 (2002) 437– 445.

[13] Monica Popa, Johannes Frantti, Masato Kakihana" Characterization of $LaMeO_3$ (Me: Mn, Co, Fe) perovskite" Solid State Ionics 154– 155 (2002) 135– 141.

[14] Monica Popa, Jose M. Calderon Moreno "Lanthanum ferrite ferromagnetic nanocrystallites by a polymeric precursor route" J. Alloys Compd. 509 (2011) 4108–4116.

[15] Jakob Andreasson, Joakim Holmlund, Christopher S. Knee, Mikael Käll, Lars Börjesson Stefan Naler, Joakim Bäckström, Michael Rübhausen Abul Kalam Azadand Sten-G. Eriksson "Franck-Condon higher order lattice excitations in the $LaFe_{1-x}Cr_xO_3$ (x=0, 0.1, 0.5, 0.9, 1.0) perovskites due to Fe-Cr charge transfer effects" Phys. Rev. B 75, 104302 (2007).

[16] Sumalin Phokha, Supree Pinitsoontorn, Santi Maensiri ,Saroj Rujirawat "Structure, optical and magnetic properties of $LaFeO_3$ nanoparticles prepared by polymerized complex method" J Sol-Gel Sci Technol DOI 10.1007/s10971-014-3383-8.

[17] Subarna Mitra, Soumen Das, Kalyan Mandal and Subhadra Chaudhuri "Synthesis of a -Fe2O3 nanocrystal in its different morphological attributes: growth mechanism, optical and magnetic properties" Nanotechnology 18 (2007) 275608.